Proceedings of 20th International Congress on Acoustics, ICA 2010

23-27 August 2010, Sydney, Australia

Rapid seafloor inversion in shallow oceans using broadband acoustic data

Adrian D. Jones (1) and Paul A. Clarke (1)

(1) Defence Science and Technology Organisation, P.O. Box 1500, Edinburgh, SA 5111, Australia

PACS: 43.30.CQ, 43.30.PC

ABSTRACT

A technique is described by which the reflectivity of the seafloor in a shallow ocean may be obtained from inversion of received broadband acoustic signals. The technique is quite general in that the source waveform may be either impulsive or quasi-continuous. The product of the inversion is the slope, F dB/radian, of the bottom loss versus grazing angle function, which is assumed linear for small grazing angles of incidence. The technique is based on a description of the spectral statistics of the multi-path interference field in a shallow ocean, and is believed to provide a rapid, but robust, estimate of reflectivity which is adequate for many uses. Examples of application of the technique to at-sea data are shown, in which comparisons are made between measurements of transmission loss and calculations which are based on the inverted parameter. It is shown how the technique may be applied across a broad frequency range, so that estimates of broadband transmission may be made. Potential limitations of the technique are discussed.

INTRODUCTION

It is well known that sound transmission in shallow oceans, including littoral and continental shelf regions, is critically dependent upon the features of the underwater environment. At low acoustic frequencies (less than about 300 Hz), or with a sound speed versus depth function which causes downward refraction, transmission to long range (30 km or more) is affected significantly by the seafloor reflective properties. Knowledge of these properties is required in order to make accurate estimates of received signal levels for all purposes, including predictions of insonification of marine fauna, the performance of undersea detection systems such as anti-submarine warfare (ASW) sonar systems, and in regard to underwater communications.

Traditionally, seafloor acoustic properties had been estimated by using available knowledge of the links to observable seafloor physical properties (e.g. grain size, porosity, material type such as sand, silt, etc.), knowledge of which were available from grabs and cores obtained during ocean research. Uncertainty exists with these processes, for many ocean regions data coverage is sparse and for almost all ocean regions knowledge of the vertical profile of the seafloor is poor. In order to supplement these estimates, and to provide seafloor acoustic data for unsurveyed locations, many techniques for acoustic inversion have been developed. Using such techniques, the seafloor acoustic properties, usually stated as the geoacoustic properties as shown in Table 1, may be determined from received acoustic data, solely.

Almost all present inversion techniques, however, do not lend themselves to rapid application due to the complexity of the measurement process, the number of sensors required, or the signal processing involved. Recently, C. H. Harrison et al. [1] described a method for the determination of seafloor reflection loss, as the bottom loss versus grazing angle parameter, F dB/radian . This was similar to the earlier published method of Smith [2], this being referenced by Harrison et al. A technique for which much of the theory is similar had been devised by Jones et al., at Maritime Operations Division (MOD), independently, and limited descriptions [3], [4], [5] had been made of this method and its application, although full details had not been published prior to the present paper.

Table 1. Seafloor Geoacoustic Parameters

compressional sound speed	c_p m/s
compressional attenuation	α_p dB/λ
shear speed	c_s m/s
shear attenuation	α_s dB/λ
density	ρ kg/m^3
sediment thickness	m

An essential feature of the methods of Harrison et al., Smith (and Jones et al.) is that the acoustic impulse response of an isovelocity shallow ocean may be used to determine the bottom loss parameter F by using the impulse decay rate. The method of Jones et al. does, however, include the ability to determine the same parameter from the spectral statistics of the frequency transfer function. In practice, this determination may be made using an acoustic impulse, but any broadband source will suffice, including coherent swept tones and random signals.

This paper describes the theory under-pinning the technique, and shows its application to rapidly sensed ocean data. Further confirmation of the effectiveness of the technique is demonstrated using inversion of synthetic data. An enticing aspect of the MOD technique is that the number of descriptive parameters is reduced (to one), whilst the ability to carry

out phase coherent transmission predictions is retained using a complementary determination of reflection phase [6].

IMPULSE DECAY FOR SHALLOW OCEAN

In what follows, the theory and relevant features of the shallow water impulse response are reviewed. The links to spectral statistics of transmission are then shown in the following section.

Impulse decay for lossless boundaries

Multi-path transmission in an isovelocity shallow ocean may be depicted by ray paths as shown in Figure 1. The transmission paths may be classified into one of four families of rays:

a) *n* surface reflections and *n* bottom reflections, with surface reflection first;
b) *n* surface reflections and *n* bottom reflections, with bottom reflection first;
c) *n* bottom reflections and *n*-1 surface reflections;
d) *n* surface reflections and *n*-1 bottom reflections.

where $n = 1$ to ∞, plus the direct arrival.

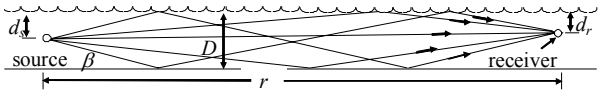

Figure 1. Multi-path transmission in isovelocity shallow ocean

For a path of type c), the source to receiver path length is

$$l_n = \sqrt{r^2 + \left[2nD - (d_s + d_r)\right]^2} \quad \text{for } n = 1 \text{ to } \infty \qquad (1)$$

where l_n is the source to receiver ray path length for ray *n*, in units of metres; *r* is the source to receiver horizontal range, m; *D* is the ocean depth, m; *n* is the index number of ray family, an integer; d_s is the source depth, m; d_r is the receiver depth, m.

In a particular family of arrivals, it may be shown that each ray arrives at time *t* after the direct arrival, given by

$$t \approx \frac{2n^2 D^2}{r c_w} \text{ seconds} \qquad (2)$$

where c_w is the speed of sound in seawater, m/s, and it is assumed that $n << r/(2D)$, that is $t << r/(2c_w)$ seconds, for which the angle of incidence of the arrival at the seafloor and ocean surface is small.

The rate of arrivals may be shown to be $r c_w / (4nD^2)$ per second. By substituting for the ray index number, *n*, in terms of time of arrival, *t*, using Equation (2), we determine that

$$\text{the rate of arrivals at time } t \text{ is } \frac{1}{2D}\sqrt{\frac{r c_w}{2t}} \text{ per second.} \qquad (3)$$

For a shallow ocean, the path length difference s_n of consecutive arrivals in the same family may be shown to be given by $s_n \approx 4nD^2/r$ metres for arrivals with small angles of incidence at the seafloor and ocean surface. As $n << r/(2D)$ for all values of interest, it follows that $s << 2D$ for all relevant arrivals, and since $r >> D$, which may be taken as a definition of "shallow", it is clear that path length differences are always very small relative to range. A direct result of this is that spherical spreading loss along any shallow angle arrival is very close to the spreading loss along the direct path, and so, in the absence of boundary losses, the shallow angle arrivals all have near-equal amplitude. The received, summed multi-path intensity as a result of an impulse will then have a decay according to the temporal density of arrivals (i.e. the arrival rate) as a function of time, from Equation (3). Clearly, this decay is most rapid at small values of *t*, and quite slow at large values of *t*.

To determine a total proportion of impulse decay to time *t*, it is necessary to assign a time t_0 as a "start" time, or reference time. Here, we make use of the fact that the time separation between arrivals, Δt_n seconds, for arrival number *n* may be given by $\Delta t_n \approx 4nD^2/(r c_w)$ seconds (see Figure 2). We may then assume that the value of Δt_n relevant to $n = 1$ will suffice for the value of t_0. By substitution into Equation (3) for this value of t_0, we get the initial rate of arrivals, and may now find a general expression for the decay of intensity following an impulse, expressed as a positive quantity in dB:

$$\text{decay of received intensity to time } t \approx 5\log\left(\frac{r c_w t}{4D^2}\right) \text{dB}. \qquad (4)$$

This expression may be termed the impulse decay due to "arrival-separation", as this is the decay following sudden cessation of insonification which is due to the increasing time separation of the successive arrivals. Note that Equation (4) is robust to errors in the estimation of the "start" time. An error by a factor of 2 amounts to an error in the estimation of the total decay by $\pm 5\log 2 \approx \pm 1.5$ dB.

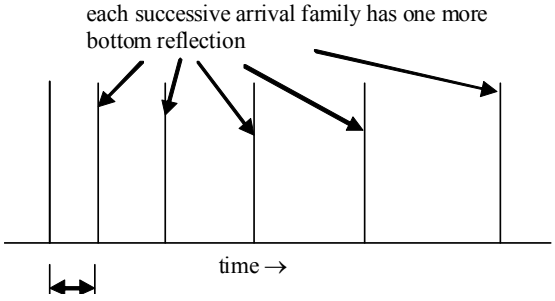

$\Delta t_n = 4nD^2/(rc_w)$, where *n* is from 1 to ∞

Figure 2. Arrival separation of ray families in impulse

Impulse decay through boundary losses

In forward transmission of a signal, we now presume that the losses at the boundaries are dominated by the loss due to reflection at the seafloor, and that there is no loss at the sea surface. For small grazing angles β, it is well established that the loss in dB on each bottom reflection may be approximated as proportional to the grazing angle, e.g. as stated by Urick [7]. The bottom loss then becomes $F\beta$ dB, where the "bottom loss slope", *F* dB/radian, is a single parameter which describes the seafloor. Weston [8], for example, showed the appropriateness of the bottom loss slope *F* in terms of bottom impedance. By comparison with full descriptions of the interference field obtained with a more conventional description of the seafloor, Jones et al. [6] showed that the assumption of a uniform bottom loss slope *F* may be used to obtain a reasonable approximation to the complete detail of the interference field.

For a shallow isovelocity ocean, it may be shown that the grazing angle β_n for a ray of index *n* in any of the four ray

families is approximately $\beta_n \approx 2nD/r$ radians for small angles. The bottom loss per bounce then follows as $2nFD/r$ dB, hence the bottom loss for all bottom interactions for ray *n*, in any ray family, follows as $2n^2 FD/r$ dB.

Substituting for *n* using Equation (2), we obtain the following expression for the bottom loss for the ray arriving at time *t* as

$$B(t) \approx c_w F t/D \text{ dB} \quad (5)$$

where $B(t)$ is the bottom loss of ray arriving at time *t*, in dB.

Now, if the arrivals are evenly spaced, that is, *if there is no arrival-separation loss*, Equation (5) represents the total rate of loss with time at the receiver, as a result of instantaneous cessation of insonification. This decay rate is uniform on a logarithmic scale, that is, the intensity at the receiver falls at an exponential rate with time *t*, described by $e^{-t/\tau}$, where τ is the impulse response time corresponding with a decay by $1/e$, that is, by $10\log_{10}(e)$ or 4.343 dB. The existence of an exponential decay to the impulse response for an isovelocity ocean with bottom loss in dB represented by a linear function in grazing angle was first shown by Smith [2]. This work was referenced, and extended, by Harrison et al. several decades later [1], [9]. Both these analyses are different to the above although the solution is the same.

The time τ for a decay by $1/e$ follows from Equation (5) as

$$\tau \approx \frac{(10\log_{10}(e))D}{c_w F} \text{ seconds} \quad (6)$$

where, as shown by Smith and Harrison et al., the result is independent of range. In Equation (1), the term $[2nD - (d_s + d_r)]^2 \approx [2nD]^2$ for values of *n* greater than about 2, regardless of source and receiver depth, and so it may be seen that Equations (2) to (5), and hence the impulse decay time τ, are effectively unrelated to source and receiver depth as well as range – a powerful result.

The time for a 60 dB decay, T_{60}, also follows from Equation (5)

$$T_{60} \approx \frac{60D}{c_w F} \text{ seconds.} \quad (7)$$

where T_{60} is time for 60 dB decay of received oceanic impulse due to bottom loss, s. Time T_{60} is related to the impulse response time, τ, as $T_{60} = 6\tau/\log_{10}(e) = 6\ln(10)\tau \approx 13.82\tau$, and is introduced here for later convenience.

In a practical transmission situation in a shallow ocean, the total decay may be regarded as the sum of the arrival-separation loss plus the bottom loss as

$$\text{intensity decay to time } t \approx 5\log\left(\frac{r c_w t}{4D^2}\right) + \frac{c_w F t}{D} \text{dB} \quad (8)$$

From Equation (8), the total decay to an impulsive input (the same as the decay following instantaneous cessation of insonification) will, initially, be dominated by the arrival-separation term, and then by the bottom loss term. In practice, at large values of time, *t*, the assumption of $t << r/(2c_w)$ seconds will fail and the decay at greater times will cease to be exponential.

The validity of the assertion, that the bottom loss term is greater than the arrival-separation term, may be seen in the examples shown in Table 2, in which the terms in Equation (7) are evaluated for several shallow ocean scenarios. These terms are evaluated for a time T_{20} corresponding with a 20 dB decay due to bottom loss, this being 1/3rd of T_{60}, as this extent of decay is typical of that which may be observed with at-sea data for which signal-to-noise is not large.

Table 2. Features of impulse decay time for isovelocity shallow oceans

Scenario	T_{20}	order *n* of family at T_{20}	arrival-separation loss to T_{20}	bottom loss to T_{20}
#1 D = 50 m r = 5 km F = 10 dB/rad	0.067 s	10	8.5 dB	20 dB
#2 D = 50 m r = 5 km F = 50 dB/rad	0.013 s	4	4.9 dB	20 dB
#3 D = 100 m r = 2 km F = 10 dB/rad	0.13 s	4	4.9 dB	20 dB
#4 D =100 m r = 2 km F = 50 dB/rad	0.027 s	2	1.5 dB	20 dB

Source: (Authors, 2010)

Data in the 3rd column of Table 2 show that for a 20 dB decay, there are at least 2 arrivals in each of the four arrival families. As this gives 8 arrivals plus the direct path, the statistics of the impulse function can be expected to be, approximately, well-behaved. That is, they will be close to the result achieved if there was a large number of arrivals. The results in the 4th and 5th columns show that the total impulse decay to T_{20} is dominated by the bottom loss, unless the bottom loss is low and the relative path lengths of the arrivals are similar due to source-to-receiver range being large or ocean depth being shallow. For greater levels of decay than 20 dB, bottom loss clearly dominates. It may also be seen from the data in Table 2 that the assumption of $t << r/(2c_w)$ seconds will not be violated by these scenarios for values of time up to T_{60} (three times the values of T_{20} shown).

A close approximation to an impulse response is obtained by the use of a small underwater explosive. Implosive devices, formed from evacuated glass vessels, for example, have also been used as impulsive underwater sound sources, as, of course, have air guns. For impulsive sound sources which have a gas residue, which includes explosives, air guns and glass vessels which are not completely evacuated, the initial impulse is followed by a smaller impulse from the collapse of the bubble of gas formed from the residue. In the case of a Mk 64 SUS (Signals Underwater Sound) explosive detonated at 60 ft, the impulse from the bubble pulse appears 0.040 seconds after the initial impulse. Regardless of source type, the signal from the bubble pulse may disturb the observation of a received impulse response, so there is value in understanding the features of the multi-path arrival structure up to the time of the first bubble pulse arrival.

The time *t* at which energy is received from the initial impulse, for any angle β_n, may be shown to be $t = \frac{l_n - r}{c_w} \approx \frac{r}{c_w}\left[\frac{1-\cos\beta_n}{\cos\beta_n}\right]$ seconds. For small grazing

angles, $t \approx r\beta_n^2/(2c_w)$, so that from Equation (2), time t within the impulse decay corresponds with the arrival of family n, where

$$n \approx \sqrt{r c_w t/(2D^2)}. \quad (9)$$

For the processing described in the following section, it is desirable to time-gate to use the pre-bubble-response section of the received waveform, only. It is desirable that the value n is not small, so that the number of arrivals ($4 \times n$) is large, and robust decay statistics are achieved.

SPECTRAL STATISTICS OF THE SHALLOW WATER ACOUSTIC INTERFERENCE FIELD

As shown by Schroeder [10] in regard to room acoustics, for a transmission environment with an exponential decay function (this assumes zero arrival-separation loss in the shallow water scenario), the autocorrelation function of the amplitude of the frequency response is very close to that for the real part of the frequency response which may be expressed as

$$\rho_{|p|}(\Delta f) = \frac{1}{\left[1+(2\pi\tau\Delta f)^2\right]} \quad (10)$$

where Δf is frequency displacement for a certain decorrelation, Hz.

As shown by Schroeder [10], this expression is derived as the Fourier cosine transform [11] of the impulse energy decay transient, the latter being effectively a power spectrum of the frequency response of the environment and, of course, an exponential. Specifically, it derives from the real, or cosine component, of the Fourier transform of $e^{-\alpha x}$ over the range 0 to ∞ (e.g. formula 1.4 (1) Page 14 of Erdélyi [12]), that is the real component of the Fourier transform of $e^{-|\alpha x|}H(x)$ where $H(x)$ is the unit step function (e.g. Page 418 of Bracewell [13]). By selecting particular values of correlation coefficient $\rho_{|p|}(\Delta f)$, the associated value of Δf may be determined from Equation (10) in terms of τ, the time for the sound intensity to decay by $1/e$.

For example, the time for a 60 dB decay may be related to the frequency displacement for the autocorrelation function to fall by 0.5 as

$$\Delta f_h = 1/(2\pi\tau) \approx 2.20/T_{60} \text{ Hz} \quad (11)$$

where Δf_h, Hz, is frequency displacement for autocorrelation function of received pressure amplitude to fall to 0.5, Δf_h being also known as the frequency variability parameter.

From Equation (11), substituting for τ using Equation (6) and the fact that $\log_{10}(e) = 1/\ln(10)$, we get

$$\Delta f_h \approx \frac{\ln(10) c_w F}{20\pi D} \text{ Hz} \approx 0.037 c_w F/D \text{ Hz}. \quad (12)$$

This expression may be inverted to obtain values for bottom loss function, F, as

$$F \approx \frac{27.3 D \Delta f_h}{c_w} \text{ dB/radian}. \quad (13)$$

If values of F are to be determined by at-sea measurements, it is advantageous to be at shorter range, rather than longer range, so long as the assumption $t << r/(2c_w)$ seconds is not violated. The reason for this is that Equation (8) shows that the component of the total impulse decay from the arrival-separation is least at short range. Under such circumstances, the "bottom loss" component will dominate for a greater time, and the statistics of amplitude variability with frequency will be more in accord with Equation (10).

Equations (12) and (13) are unique to the present analysis. This result is significant as it enables the construction of a number of viable techniques of sampling spectral variability, and thus inverting the value of bottom loss function, F, whereas the techniques implied by the analyses of Smith [2], and Prior and Harrison [1], are restricted to the generation and observation of an oceanic impulse. The method of Equations (12) and (13) may be carried out using a variety of broadband signal types and does not require transients.

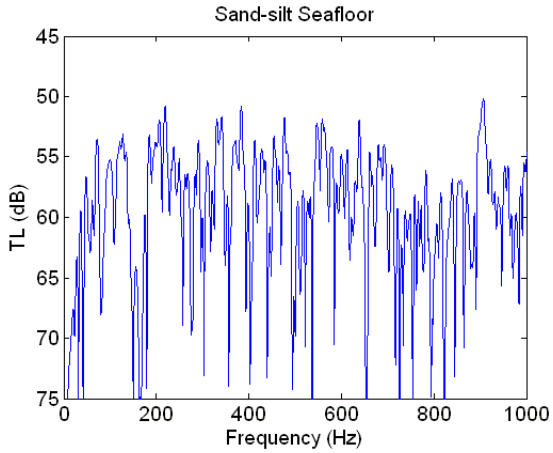

Figure 3. *TL* versus frequency at range 3000 m for ocean of depth 80 m, source and receiver at 18.3 m depth

Figure 3 shows an example of phase-coherent *TL* versus frequency for a shallow, isovelocity, ocean as determined by a ray model, for source and receiver depth both 18.3 m (60 ft), ocean depth 80 m and source to receiver range 3000 m. In this case the seafloor was modelled as a uniform half-space, with the geoacoustic parameters as for the sand-silt seafloor specified by Jensen and Kuperman [14]. For these parameters the seafloor reflection coefficient versus grazing angle function, as shown in Figure 4, is independent of frequency.

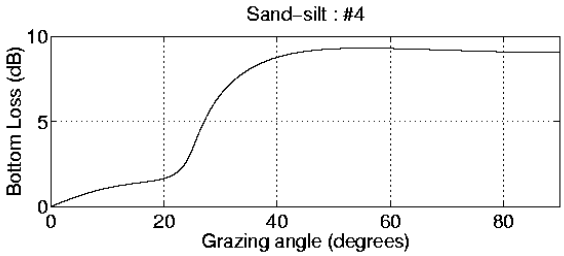

Figure 4. Bottom loss versus grazing angle for Jensen & Kuperman [14] sand-silt seafloor

The data in Figure 4 show a near-uniform rise in bottom loss with grazing angle to about 20° which, in this case, corresponds with the critical angle. For transmission in a shallow ocean, the bottom loss at small grazing angles is significant, and a value of F may be estimated from this data below the critical angle: $F \approx 6$ dB/radian. From Equation (12), this results in a value of $\Delta f_h \approx 4$ Hz. By eye, these values are consistent with the fine-scale features in the data in Figure 3.

As the bottom loss is frequency-independent for this seafloor, it may be noted that the corresponding multi-path arrivals have the same amplitude regardless of frequency, and differ merely in phase. It may then be argued that the amplitude of the phase-coherent sum has Rayleigh statistics, and that the phase-incoherent *TL* will be frequency independent. In fact, if the values near 0 Hz are excluded, as these correspond with an amplitude null (values below 100 Hz were excluded), the standard deviation of the amplitude values, in dB, is 5.54 dB, very close to the $\sigma = 10\left(\pi/\sqrt{6}\right)\log_{10}(e) \approx 5.57\text{dB}$ expected for a Rayleigh distribution (e.g. equation (2) of Schroeder [15]).

Independence of transmission samples

Frequency displacement Δf_h is indicative of that required for a significant change in received signal amplitude level. However, an alternate quantity, a frequency displacement Δf_i for statistical independence of received signal amplitude levels, may be obtained, based on Schroeder's considerations [15] of the standard deviation of the averaged sound pressure amplitude, in dB, of signals received across a frequency band.

As outlined in the previous section, for a highly multi-modal transmission situation, received pressure amplitude values are Rayleigh distributed with frequency, and the envelope of these values expressed on a logarithmic scale (as dB SPL), has a standard deviation, $\sigma \approx 5.6$ dB. From Schroeder [15], the standard deviation, σ_B, of the frequency-averaged logarithmic response is reduced as a function of $B\times\tau$ or $B\times T_{60}$, where B is the averaging bandwidth, and becomes:

$$\sigma_B \approx \frac{5.6}{\sqrt{1+3.3\tau B}} \approx \frac{5.6}{\sqrt{1+0.238 T_{60} B}}\text{dB}. \qquad (14)$$

These reduced fluctuations may be considered to be the result of averaging over N independent measurements. In a general sense, the standard deviation σ of a sample from a distribution which itself is formed from the sum of samples from N distributions, each of which has a standard deviation σ_a, is $\sigma_a/\sqrt{N}$, as is well known. Thus, in the present case, we expect that averaging over N independent samples will reduce the standard deviation to $\sigma_B = 5.6/\sqrt{N}$ dB. Then, from Equation (14), frequency averaging corresponds with making $1+3.3\tau B$ (or $1+0.238 T_{60} B$) independent measurements. Frequency spacing for independence then corresponds with the minimum value of B which gives two independent samples. The frequency separation Δf_i for independence of spectrally sampled received signal amplitude levels in dB is then

$$\Delta f_i \approx \frac{1}{0.238 T_{60}} \approx \frac{4.2}{T_{60}}\text{Hz}. \qquad (15)$$

We note from Equations (15) and (11) that $\Delta f_i \approx 2\Delta f_h$, which makes for a convenient approximation. In practice, T_{60} will be frequency dependent, but Equations (11) and (15) are valid so long as the values of Δf_h and Δf_i are small compared with the frequency range over which T_{60} changes. We may also express Δf_i in terms of the environmental parameters, as

$$\Delta f_i \approx \frac{\ln(10) c_w F}{33 D}\ \text{Hz} \approx 0.070\, c_w F/D\ \text{Hz}. \qquad (16)$$

The number of independent samples N is then given by

$$N \approx 1+3.3\tau B \approx 1+0.238 T_{60} B. \qquad (17)$$

Substituting for τ from Equation (6), we get

$$N \approx 1+\left[14.3\, D\, B\right]/\left(c_w F\right). \qquad (18)$$

In general, there are two degrees of freedom associated with each independent sample, so the number of degrees of freedom is simply double the number N. The concept of the number of independent spectral samples has implications that are beyond the scope of the present paper, however, it is clear that a value of Δf_h may not be well resolved unless the spectral band includes multiple degrees of freedom.

Implications of Lloyd's Mirror

Strictly, the direct path does not feature in the above statistical derivations. Its effect, relative to that of the 4 arrivals of each of the first arrival families, is assumed to be insignificant. In the case of a highly absorbing seafloor, the direct path arrival will undergo interference with the arrival with just one surface reflection, and no other arrivals are significant. The resulting pattern of nulls and enhancements is the well-known Lloyd's mirror interference (e.g. Urick [16], page 131). The Lloyd mirror geometry is shown in Figure 5.

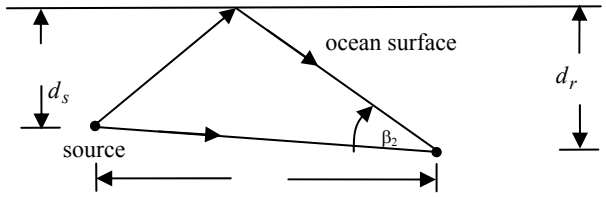

Figure 5. Lloyd's mirror geometry

Strictly, if the frequency variation due to random multi-path effects is to be observed (e.g. to determine values of Δf_h from an at-sea measurement), the Lloyd's mirror frequency pattern should be determined and removed from the spectrum of received sound. For each scenario, there is a null at 0 Hz, with subsequent nulls at frequencies given as follows:

$$\text{intensity nulls at } f = \frac{n\, c_w\, r}{2\, d_s\, d_r} \text{ for } n = 0, 1, 2, 3 \ldots . \qquad (19)$$

In practice, apart from the null at 0 Hz, the Lloyd's mirror pattern is not greatly evident in spectra of signals received at ranges for which seafloor grazing angles are small. An illustration of the extent of the "overlay" of the Lloyd's mirror pattern is shown in Figure 6. This shows the *TL* versus frequency for the same depth of ocean and source to receiver range used for Figure 3, but for a clay-silt seafloor [14]. Also shown, by a dashed line, is the *TL* versus frequency for a completely absorbing seafloor, thus representing Lloyd's mirror for the same scenario.

The bottom loss versus grazing angle function for the clay-silt seafloor is shown in Figure 7. A value of F estimated from the data below about 15° grazing angle gives $F \approx 37$ dB/radian. From Equation (12), this results in a value of $\Delta f_h \approx 26$ Hz, which by eye, is consistent with the fine-scale data for the clay-silt seafloor shown in Figure 6. The Lloyd's mirror data shows nulls, as expected from Equation (19), whereas the corresponding data for the clay-silt seafloor shows nulls that are much less pronounced and not always at the same frequencies. The data for the clay-silt seafloor have the appearance of being Rayleigh distributed, and may be shown to have a standard deviation σ = 5.78 dB, very close to the 5.57 dB expected for Rayleigh, whereas for

data corresponding to Lloyd's mirror, a larger standard deviation σ = 7.9 dB may be shown to be expected.

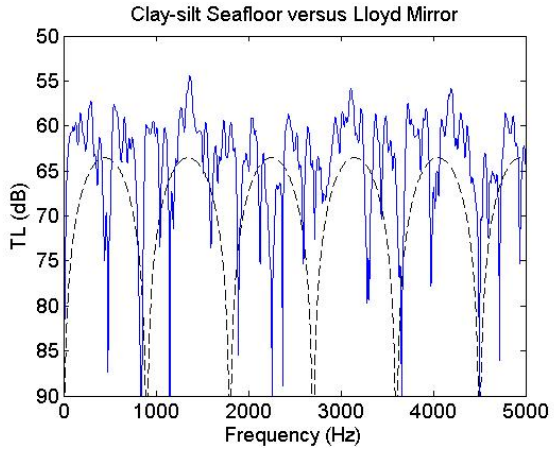

Figure 6. *TL* vs. frequency at range 3000 m for ocean of depth 80 m, source and receiver at 50 m depth

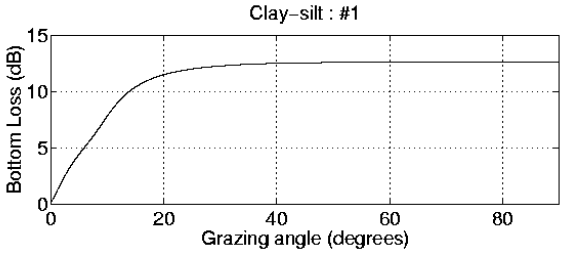

Figure 7. Bottom loss versus grazing angle for Jensen & Kuperman [14] clay-silt seafloor

This exercise was repeated for a seafloor consisting of a calcareous ooze (p 462 of ref. [17]) half-space, to represent a highly absorbent seafloor. The data are shown in Figure 8. Clearly, the Lloyd's mirror pattern is more evident than in Figure 7, although it is still not dominant.

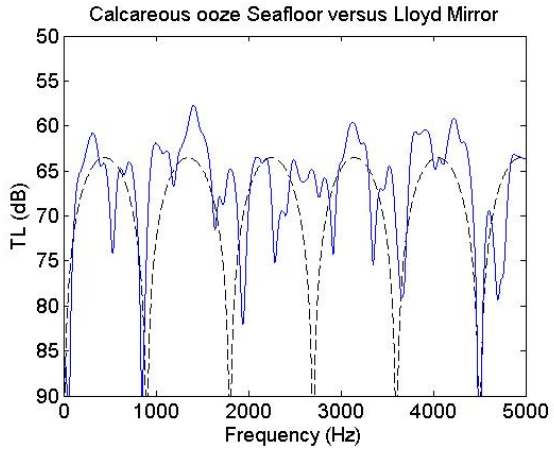

Figure 8. *TL* vs. frequency at range 3000 m for ocean of depth 80 m, source and receiver at 50 m depth

Implications of low frequency

The analysis developed in this paper is based on the appropriateness of ray theory for the description of the received impulse decay and for the variation of *TL* with frequency. At frequencies which are too low for ray theory to be valid, the transmission may be considered as occurring through a combination of propagating modes and evanescent modes, with few modes existing. Apart from any more detailed considerations, however, a low frequency limit f_l may be seen to exist when the path length difference between arrival families is small relative to a wavelength, λ. In these cases, and for all lower frequencies, there will be a near cancellation of the total received signal, as those arrivals that have odd numbers of bottom reflections will be nearly π radians out of phase with those that have even numbers of bottom reflections. The detailed nature of the seafloor reflection will be relevant, but the near-cancellation can be seen to occur regardless, below the limiting frequency f_l.

This near-cancellation of the received signal may be seen to occur if the path length difference between the 1st and 2nd arrival families is less than, very approximately, about $\lambda/8$ metres (The cancellation caused by an arrival and its surface reflection which is π radians out of phase plus Δλ different in length may be shown to be $20\log(\sin[\pi\,\Delta\lambda/\lambda]) \approx 8.3$ dB for $\Delta\lambda = \lambda/8$.). From Equation (1), this length difference $l_{n=2} - l_{n=1} \approx 6D^2/r$ metres, so that the near-cancellation occurs for frequencies less than about $f < \frac{r c_w}{48 D^2}$ Hz. For example, for the scenario of Figure 3, near-cancellation of arrivals may be expected for frequencies lower than about 15 Hz, which is in approximate agreement with the data in the figure.

APPLICATION TO RAPID SEAFLOOR INVERSION IN SHALLOW OCEANS

The MOD technique is based on the receipt of broadband signals at medium ranges (r = 2 to 4 km approximately), and the omni-directional summation of all multi-path arrivals at a single receiver. The rate of variability of the received signal amplitude, as a function of frequency, is related to the (average) speed of sound in seawater, the ocean depth and the seafloor bottom loss versus grazing angle parameter F dB/radian. By inverting the relationship, by use of Equation (13), the seafloor bottom loss versus grazing angle function may be estimated to an accuracy sufficient for many acoustic transmission modelling purposes. The inversion technique assumes multi-path transmission with no refraction of ray-paths, however, it has been found that for the short measurement ranges used, any ocean refractive effects have a minimal impact on the inverted parameter returned by the technique. Advantages of the technique are that source to receiver range need not be well known, neither source nor receiver depth need to be known, and the response of neither source nor receiver need be calibrated. The few disadvantages include the need for the seafloor to be without slope, and the fact that the technique returns a total boundary loss for received coherent signals, which will include losses due to surface and seafloor roughnesses. Recent research of boundary losses (e.g. Williams et al. [18]) suggests that the shallow angle loss-versus-grazing-angle function from roughness effects is linear in dB, thus resembling the seafloor absorptive loss function F. This suggests that sea surface roughness losses might be removed from the total measured loss to yield a combined seafloor loss due to absorption plus roughness. In what follows, roughness losses are neglected.

In application, the key aspect is the determination of the spectral variability parameter, Δf_h, this being the frequency displacement at which the normalised autocorrelation of the amplitude of the sound channel frequency response, $\rho_{|p|}(\Delta f)$, falls to 0.5. After Schroeder [10], this normalised autocorrelation is carried out as

$$\rho_{|p|}(\Delta f) = \frac{\langle |p(f)||p(f+\Delta f)| \rangle - \langle |p(f)| \rangle^2}{\langle |p(f)|^2 \rangle - \langle |p(f)| \rangle^2} \quad (20)$$

where the autocorrelation is carried out on the zero-mean sound pressure modulus, that is, on $|p(f)| - \langle |p(f)| \rangle$. For practical implementations of the technique, either an impulsive transient, swept tone, or random signal source may be used.

Example application - features of at-sea data

Data used for this present purpose were obtained by DSTO in 1990. The at-sea trial was carried out for other purposes, and the data were subsequently re-analysed. In the trial, impulse response data were obtained using a suitable receiver located at 18.3 m depth from a surface buoy, while small explosives (small SUS charges) were deployed from a ship as it moved away to a range of about 30 km. Each SUS charge was set to detonate at 18.3 m depth. Ocean depths were obtained continuously, using a ship-based high-frequency echo sounder, and were found to be uniform to a reasonable approximation along the track. Surficial sediment samples were obtained at the start of the track. Two bathythermograph recordings were made, from which sound speed variation with depth was determined.

Time series of sound pressure arrivals were selected for analysis only for those waveforms for which the measured peak excursion pressure was at least 5.5 dB less than the hard-clipping limits of the recording system. Here, the recording system specifications accounted for individual sonobuoy characteristics. This criterion was chosen as it exceeded the maximum possible amount by which the assumed waveform of the initial peak (an instantaneous rise, followed by an exponential decay with time constant about 0.1 ms) might be underestimated due to the digital sampling rate of 20 kHz, and anti-alias filtering at 8 kHz, which were employed. This process ensured that any impulsive waveform selected for study was recorded appropriately.

Data for Track A

The SSPs (sound speed profiles) at the start and at the end of the Track A are shown in Figure 9. These SSPs are indicative of downward refraction for which significant acoustic interaction with the seafloor is expected. Further, as source and receiver were at 18 m, these profiles indicate that the surface ducting conditions, which are strongly linked to high frequency transmission phenomena, were likely to be highly variable along the track, and that in retrospect, the two sets of sound speed data were insufficient to describe the range-dependent refraction conditions which clearly existed.

A ray diagram prepared for Track A, using the BELLHOP model, is shown in Figure 10. This has been prepared to include those rays launched at elevation angles commencing at 0.0 degrees and at 0.5 degree increments to ± 2½ degrees. The observed ocean depth and sea surface data is shown in Table 3. The pressure waveform received at 2.2 km is shown in Figure 11, with the detail of the initial part of the waveform being shown in Figure 12.

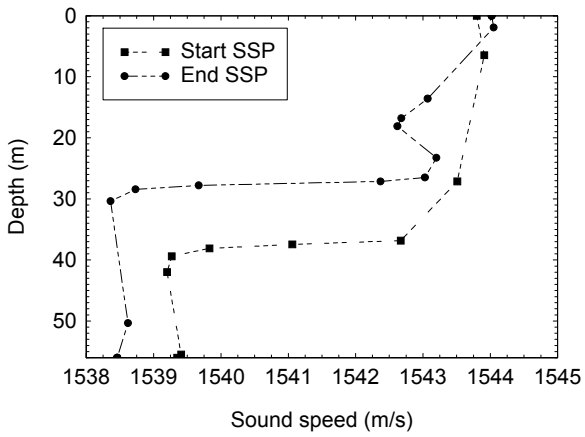

Figure 9. Sound Speed Profiles at start and end of Track A

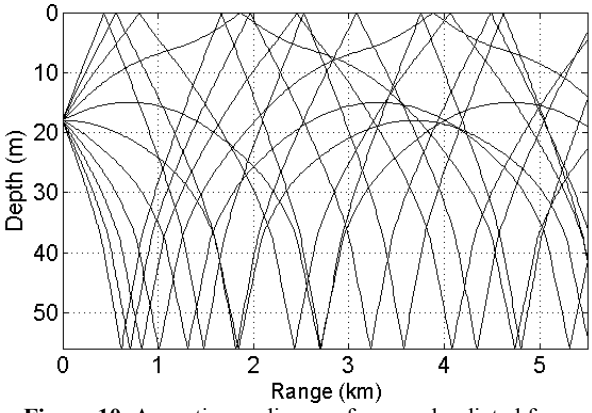

Figure 10. Acoustic ray diagram for sound radiated from source for Track A, 11 rays over ± 2½ degrees

Table 3. Ocean depth and sea surface data for Track A

Ocean depth (m)	Wind speed (m/s)	Swell height (m)
58 - 65	1	0

Source: (DSTO)

Historical description of seafloor for Track A

A seafloor database had the description shown in Table 4 [5]. The *in-situ* measurement accompanying the 1990 at-sea trial described the sediment as sand-silt-clay. This description, and the values within Table 4, are consistent with the mean grain size $\phi = 6.4$ as determined from a sediment sample at the start of the track.

Table 4. Seafloor Parameters for Track A from database

compressional sound speed	c_p	1570 m/s (m)
compressional attenuation	α_p	0.172 dB/λ
density	ρ	1660 kg/m^3
sediment thickness		259 m

Source: (DSTO)

Transmission Loss (*TL*) data predicted using the RAM model [19], and using the above input parameters, is presented in Figures 14 to 16.

Seafloor reflectivity from inversion technique

The MOD inversion technique requires a determination of the frequency variability of transmission, for a scenario involving shallow grazing angles at the sea surface and seafloor. For Track A, for which ocean depth was about 60 m, a suitable sound source was the Mk 64 SUS deployed at 2.2 km range, as shown in Figure 11. The section of the derived broadband

spectrum to 800 Hz is shown in Figure 13. Note that this has been based on the 40 ms of data which includes the initial arrivals and precedes the section of the signal containing the bubble pulses. The bubble-pulse section has been excluded from this analysis as it generated spectral components associated with the bubble harmonics and its inclusion might have affected the determination of what would otherwise be the true oceanic transfer function. From the analysis given in an earlier section, the period of 40 ms permits inclusion of families of arrivals with up to 4 bottom bounces, sufficient for the oceanic transfer function to be defined.

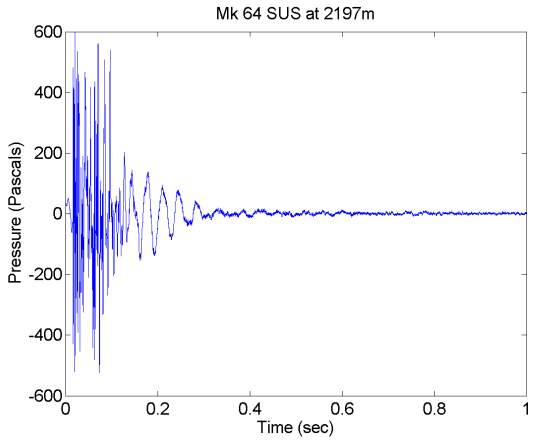

Figure 11. Received sound pressure time series, Track A, full pulse, 2.2 km

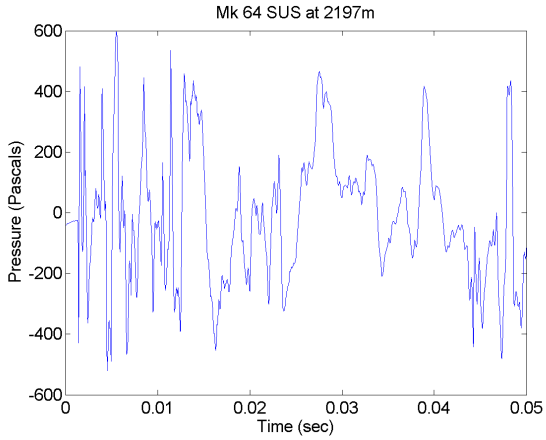

Figure 12. Received sound pressure time series, Track A, initial 0.05 s, 2.2 km

The data shown in Figure 13 were processed using Equation (20) to determine the spectral variability parameter Δf_h for each octave band of frequencies. Based on these values, the MOD inversion technique, Equation (13), was used to derive the values of bottom loss versus grazing angle, as dB/radian, for the different octave ranges. Initial derived values were [5]: 6.57 dB/radian for 125 Hz octave band, 6.52 dB/radian for 250 Hz band and 8.52 dB/radian for 500 Hz band. These values, together with an assumed relationship for reflection phase angle [6], were used as inputs to an associated DSTO process that yielded a set of parameters for a fluid seabed which had an equivalent acoustic effect at shallow grazing angles. These derived geoacoustic parameters were, in turn, used as inputs to the RAM model and used with ocean depth data and measured sound speed data to obtain long-range *TL* values. The predictions of transmission loss so obtained are shown in Figures 14, 15 and 16 by a bold dashed line.

A practical aspect of the implementation of the inversion from the data in Figure 13 is that there needs to be sufficient variation in signal amplitude over the frequency span of an octave for a value of Δf_h to be extracted with confidence. For practical purposes, the sound pressure samples, in dB, across an octave, were regarded as needing a standard deviation not far from the 5.6 dB expected for Rayleigh statistics. For the present data for Track A, this limited the DSTO technique to the octave centred at 125 Hz.

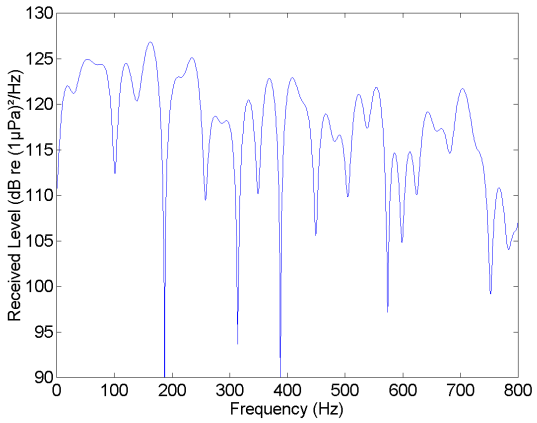

Figure 13. Spectrum from first 0.04 s of impulse, Track A, 2.2 km

Subsequent to the initial analysis carried out in 2002 [5], a re-analysis was carried out using a revised implementation of the above technique, with results as shown in Table 5. These show similar results for the same SUS (at 2.2 km range) but show a variation for the SUS at 3.4 km. A potential issue may be the added effect of refraction to the longer range. These differences are not considered further in this paper.

Table 5. Features of seafloor inversion for Track A

Frequency (Hz)	Inverted bottom loss function *F* dB/radian	
	SUS at 2.2 km	SUS at 3.4 km
125	6.9	10.9
250	7.2	10.1
500	8.5	7.0
1000	17.7	11.0
2000	20.2	23.3
4000	31.6	58.9
range/depth ratio	37	57

Source: (Authors, 2010)

TL from inverted seafloor vs. measurement

TL measurements obtained using the received Mk 64 SUS charge signals gathered during the DSTO trial are given in Figures 14, 15 and 16 for 1/3rd octave bands centred at 125 Hz, 250 Hz and 500 Hz, respectively. Three-way comparisons have been carried out between: (i) these *TL* data measured at specified ranges; (ii) *TL* predicted using the RAM model with seafloor data from an historical database (Table 4) labelled "Seafloor Database"; (iii) *TL* predicted by DSTO using the RAM model with the seafloor described as a fluid which gives the equivalent reflectivity to the values inverted at shallow angles of incidence (bold dashed line). These inverted seafloor reflectivity values are those obtained initially for the SUS at 2.2 km range, not the slightly different values shown in Table 5. The last predictions used the SSP at the start of the track; predictions based on the seafloor database used the start SSP to 15 km and the end SSP from 15 km to 30 km. For ease of comparison with the measured 1/3rd octave *TL* data, the last predictions were each obtained

by averaging *TL* values obtained at 21 frequencies equi-spaced over each respective 1/3rd octave. Here, the single frequency data were averaged using incoherent summation at 100 m range intervals. The *TL* data based on the seafloor database are from a phase-coherent calculation at the single frequency corresponding with the centre of each respective band.

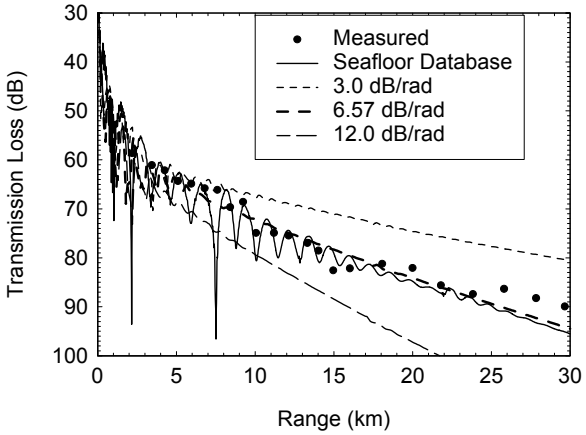

Figure 14. *TL* measured & predicted, Track A, 125 Hz

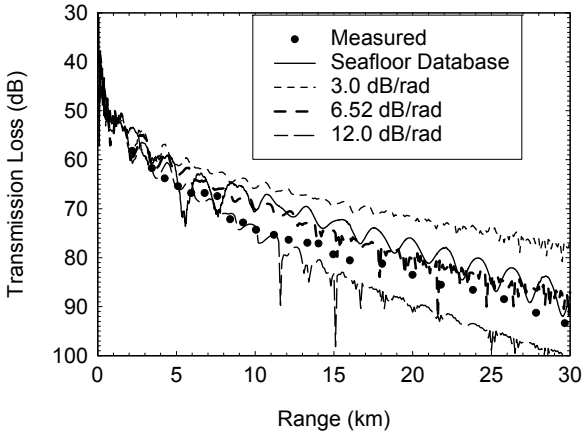

Figure 15. *TL* measured & predicted, Track A, 250 Hz

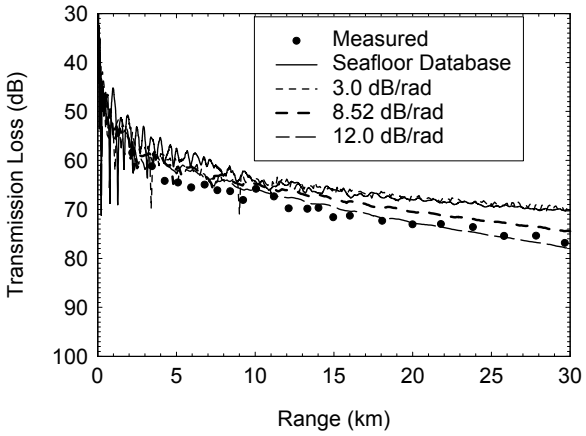

Figure 16. *TL* measured & predicted, Track A, 500 Hz

The data in Figures 14, 15 and 16 show very good agreement between measured *TL* values and the data predicted using the DSTO inverted seafloor reflectivity and do seem to imply that the DSTO technique works well for this site. The *TL* predictions based on the seafloor database are accurate at 125 Hz, but slightly further from the measurement at 250 Hz and 500 Hz. This generally good agreement is presumed due to the fact that a reasonable quantity of seafloor data for this site exists in the historical record.

In order to illustrate the sensitivity of the derived *TL* data to errors in the inversion of seafloor reflectivity, predictions of *TL* were made for values of seafloor reflectivity parameter *F* of 3 dB/radian and 12 dB/radian. These predictions are shown in Figures 14, 15 and 16 with thin dashed lines. Clearly, at the lower frequencies of 125 Hz and 250 Hz, a correct description of seafloor reflectivity is critical to accurate *TL* predictions for this ocean scenario.

INVERSION WITH SYNTHETIC DATA

To further illustrate the effectiveness of the spectral variability inversion technique, the process was demonstrated with synthetic data. Here, simulations [3] were used to determine the ocean transfer function for a short range, shallow water environment with, alternately, a seafloor with an absorptive and a reflective basement. These transfer functions were then used to determine a value for the frequency variability parameter Δf_h from which a bottom loss versus grazing angle function F dB/radian was inferred for shallow grazing angles.

The standard transmission scenario was as follows: source depth 18.3 m, receiver depth 18.3 m, ocean depth 80 m, isovelocity ocean with sound speed 1500 m/s. Both the seafloor and the ocean surface were assumed to be smooth. Two seafloor types were modelled: one with an absorptive chalk-limestone basement [14], the other with a reflective basement (Jiang type D [20]). For each seafloor type, the basement half-space was overlaid with a sediment layer. Sediment layer thicknesses and geoacoustic properties chosen for these seafloor types are given in Figures 17 and 18. Transmission simulations were carried out across the frequency range 40 Hz to 750 Hz, so that simulations might cover octave bands from 63 Hz to 500 Hz. The transmission model used for this purpose was the wavenumber integration model OASES version 2.1 [21]. *TL* values were obtained for omni-directional transmission and reception over a horizontal range of 4 km.

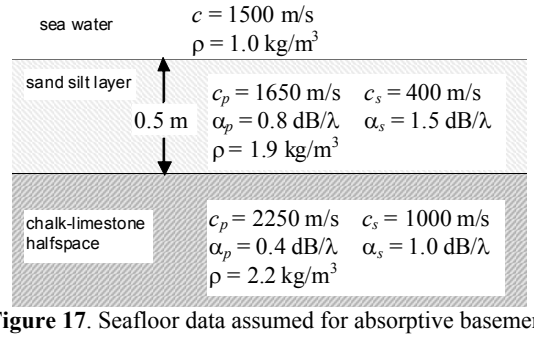

Figure 17. Seafloor data assumed for absorptive basement

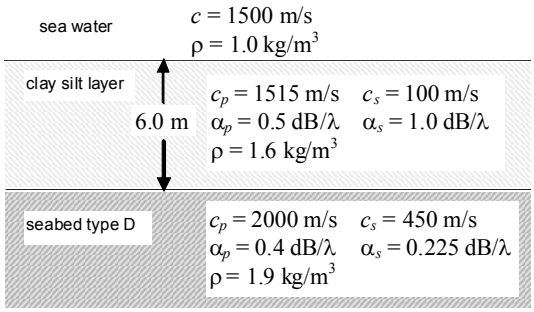

Figure 18. Seafloor data assumed for reflective basement

The properties of the sediment layers were chosen so that the overall effect of each seafloor would change with frequency. The absorptive basement was overlaid with a reflective layer of sand-silt [14]. By choosing a sediment thickness of 0.5 m,

the reflectivity of the resultant seafloor at shallow grazing angles varied from absorptive at 63 Hz, to reflective at 500 Hz. Conversely, the reflective sediment was overlaid with a layer of absorbing clay-silt [14]. Here, a sediment thickness of 6.0 m gave reflective properties at shallow grazing angles at 63 Hz, but absorptive properties at 500 Hz.

Figures 19 and 20 give the bottom loss versus grazing angle functions determined for the seafloor types depicted in Figures 17 and 18. These estimations were obtained using a plane wave reflection model prepared at DSTO using established theory [22]. In each of these figures, the data at shallow grazing angles (0º to 15º approx.) do appear to represent a near linear rise in bottom loss with angle, for each seafloor type. Further, the values of bottom loss versus grazing angle F dB/radian derived from the shallow angle data in Figures 19 and 20 do depict a progression with frequency from absorptive to reflective properties, and vice versa, respectively. These data, obtained from the average slope over the grazing angles from 0º to 10º, are shown in Table 6.

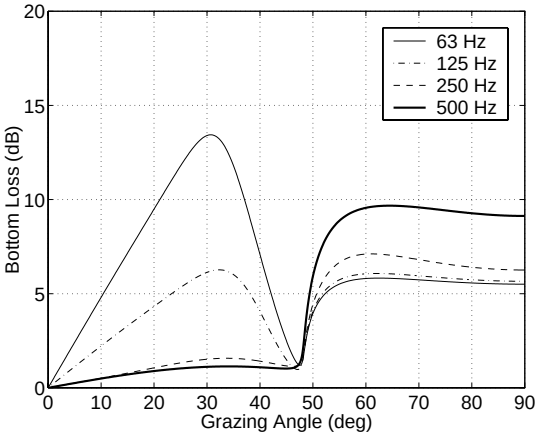

Figure 19. Bottom Loss versus grazing angle for seafloor with absorptive basement

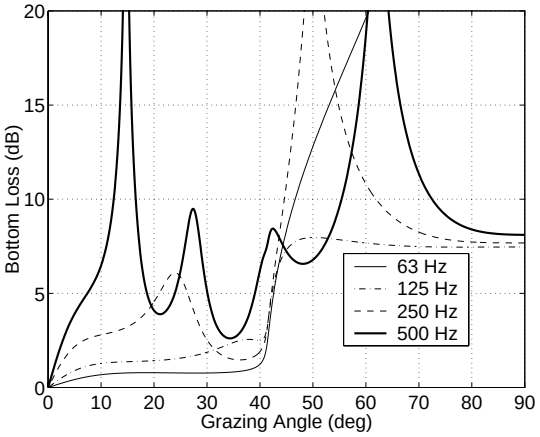

Figure 20. Bottom Loss versus grazing angle for seafloor with reflective basement

Table 6. Bottom Loss function based on grazing angles 0º - 10º - derived from Figures 19, 20

Seafloor with Absorptive Basement		Seafloor with Reflective Basement	
Frequency Hz	Reflectivity F db/radian	Frequency Hz	Reflectivity F db/radian
63	27.5	63	3.7
125	12.6	125	7.4
250	2.9	250	16.0
500	2.9	500	37.2

Source: ([3], 2000)

Inversion result

For each of the two seafloor types, the OASES predictions of *TL* versus frequency were transformed into values of signal level received, versus frequency. The sound source was assumed to have the same, arbitrary, source level at all frequencies. The received signal level data across each octave band was then processed using Equation (20) to obtain the frequency variability parameter Δf_h, and the bottom loss versus grazing angle value F dB/radian was obtained using Equation (13) for each frequency band for both seafloor types. The values of F dB/radian which were obtained in this way, are shown in Table 7.

Table 7. Bottom Loss function derived from received signal level data at 4 km range

Seafloor with Absorptive Basement		Seafloor with Reflective Basement	
Frequency Hz	Reflectivity F db/radian	Frequency Hz	Reflectivity F db/radian
63	18.8	63	2.1
125	11.6	125	7.6
250	6.3	250	38.7
500	7.2	500	30.8

Source: ([3], 2000)

The values for the inverted bottom loss function F shown in Table 7, are, in general, in good agreement with the data obtained for shallow grazing angles via the plane wave reflection model shown in Table 6. The agreement is less satisfactory in some instances – in particular, the bottom loss inferred at 250 Hz for the reflective basement. It is possible that this may be due to the fact that the data in Table 6 obtained from Figure 20 were averaged over grazing angles 0° to 10°, whereas the slope of the 250 Hz line in Figure 20 varied over this range. From Figure 20, at 250 Hz, the slope at 2º (32 dB/radian) is close to the value of 38.7 dB/radian inverted at 4 km range. From the expression $\beta_n \approx 2nD/r$ (given in an earlier section), for the arrival angle β_n for arrival family n, we see that there are $n \approx 2$ arrival families, giving 8 arrivals plus the direct path, at about 4°. These arrivals may have influenced the return from the inversion, implying that, in this case, averaging bottom loss slope over the first 10° may have given inappropriate values.

Predictions of Transmission Loss

The inverted seafloor reflection data shown in Table 7 were used as input to calculations of *TL* to long range (50 km). Here, it was assumed that the bottom loss rose linearly with grazing angle, at the slope given by the relevant value of dB/radian shown in Table 7, to the grazing angle of 20º. For all higher values of grazing angle, the bottom loss was assumed constant at the value achieved at 20º. To simplify calculations, the seafloor reflection phase angle was assumed to be the same for all grazing angles. (Note that the DSTO technique of application of inverted bottom loss and reflection phase is now slightly different [6], although the impact on these *TL* predictions is believed small.) These assumed bottom loss and phase angle data were then supplied as direct input to the KRAKEN transmission model [23]. Sample *TL* predictions so obtained are shown in Figure 21 for frequencies of 63 Hz and 125 Hz (note: data for 63 Hz have greater *TL* than that for 125 Hz) for the seafloor with the absorptive basement, and in Figure 22 for 500 Hz for the seafloor with the reflective basement. These predictions are shown com-

pared with those obtained by using the KRAKEN model in the conventional way, with the sediment and the half-space represented by the geoacoustic parameters shown in Figures 17 and 18. For these predictions, the ocean depth is assumed to be 80 m, and source and receiver are both at 18.3 m depth, and an isovelocity SSP is used.

The data in Figures 21 and 22 do show that the predictions of long range *TL* obtained by the use of the inverted seafloor properties are in reasonable agreement with those obtained by a full description of the wave propagation in the sediment and basement layers. These phase-coherent predictions of *TL* do not agree in all the detail of the fluctuations with range, but do agree well in terms of overall level.

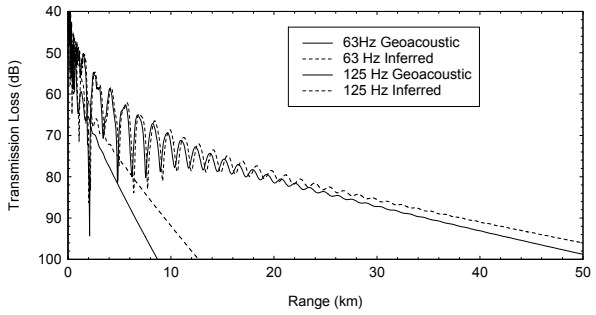

Figure 21. *TL* for absorptive basement, isovelocity ocean

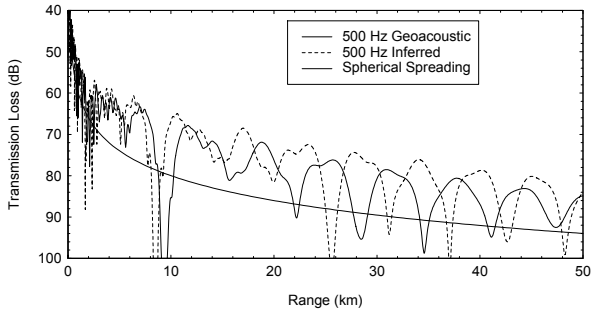

Figure 22. *TL* for reflective basement, isovelocity ocean

CONCLUSIONS

The paper presents a new technique for the inversion of the seafloor reflectivity parameter, *F* dB/radian, for application to shallow ocean environments. The theoretical derivation of the technique is presented, and the links to the previously published method of Smith, and Prior and Harrison are shown. Essentially, the present technique includes the earlier method, but is based on the spectral equivalent of the channel impulse response of the other. It is believed that the subsequent inversion of the seafloor reflectivity parameter, using data received across a frequency band, presents a great improvement in utility over the need to use an impulsive sound source.

The practical application of the technique to existing broadband at-sea data has been illustrated using data received from small explosive changes. It is shown that Transmission Loss versus range data, generated using the inverted data, is a good match to at-sea measurements. The application of the technique is further demonstrated by the use of synthetic data. In this case, the technique worked well to resolve the seafloor reflectivity parameter for seafloors for which the reflective properties were known to vary across the frequency range, due to the variation in the penetration of sound through the surficial layer of sediment into a basement of different properties.

Although all potential measurement arrangements have not been outlined in this paper, it does seem that the inversion by means of determination of the frequency variability parameter, Δf_h, offers great scope for rapid inversion by any one of a variety of techniques, and also that potential exists for reprocessing of data captured for other purposes. It is acknowledged that the technique has a number of limitations, and these are described in the paper. Notwithstanding these, it does appear that the inverted seafloor reflectivity values, obtained using the technique, were sufficient for input to acoustic transmission predictions of good accuracy, particularly at lower frequencies (under about 500 Hz) for which knowledge of the seafloor presents the greatest challenge.

ACKNOWLEDGEMENT

The authors acknowledge the efforts of DSTO staff members who collected, processed, archived and documented the data used in this paper, in particular, Dr. M. V. Hall.

REFERENCES

1 M.K. Prior and C.H. Harrison, “Estimation of seabed reflection loss properties from direct blast pulse shape”, *J. Acoust. Soc. Am.,* **116** (3), 1341 – 1344 (2004)

2 P.W. Smith, Jr. “The averaged impulse response of a shallow-water channel”, *J. Acoust. Soc. Am.,* **50**, 332 – 336 (1971)

3 A.D. Jones, D.W. Bartel, P.A. Clarke and G.J. Day, “Acoustic Inversion for Seafloor Reflectivity in Shallow Water Environment”, *Proceedings of UDT Pacific 2000*, Darling Harbour, Australia, 7-9 February (2000)

4 A.D.Jones, J.Hoffman and P.A.Clarke, “Seafloor Reflectivity – A Test of an Inversion Technique”, *Proceedings of Australian Acoustical Society Annual Conference 2000*, Joondalup, Western Australia, 15 – 17 November (2000)

5 A.D. Jones, J.S. Sendt, Z.Y. Zhang, P.A. Clarke and J.R. Exelby, “Optimisation of Transmission Predictions for a Sonar Performance Model for Shallow Ocean Regions”, *Proceedings of Australian Acoustical Society Annual Conference 2002*, Adelaide, South Australia, pp 71-80, 13 – 15 November (2002)

6 A.D. Jones, G.J. Day and P.A. Clarke, “Single parameter description of seafloors for shallow oceans”, *Proceedings of Acoustics’08 Paris*, Paris, France, 29 June – 4 July 2008, pp 1725 – 1730, also published in *Proceedings of the 9th European Conference on Underwater Acoustics, ECUA 2008*, Volume 1, pp 161 – 166 (2008)

7 R.J. Urick, “Intensity Summation of Modes and Images in Shallow-Water Sound Transmission”, *J. Acoust. Soc. Am*., **46**, No. 3 (Part 2), 780-788 (1969)

8 D.E. Weston, “Intensity-Range Relations in Oceanographic Acoustics”, *Journal of Sound and Vibration*, **18** (2), 271-287 (1971)

9 C.H. Harrison and P.L. Nielson, “Multipath pulse shapes in shallow water: Theory and simulation”, *J. Acoust. Soc. Am.*, **121** (3), 1362–1373 (2007)

10 M.R. Schroeder, “Frequency-Correlation Functions of Frequency Responses in Rooms”, *J. Acoust. Soc. Am.*, **34**, No. 12, 1819-1823 (1962)

11 M.R. Schroeder and B.S. Atal, “Generalised Short-Time Power Spectra and Autocorrelation Functions”, *J. Acoust. Soc. Am.*, **34**, No. 11, 1679-1683 (1962)

12 A. Erdélyi, Ed., *Tables of Transform Integrals, Volume I*, (McGraw-Hill Book Company, Inc. New York 1954)

13 R.N. Bracewell, *The Fourier Transform and its Applications*, 2nd edition revised, (McGraw-Hill Book Company 1986)

14 F.B. Jensen and W.A. Kuperman, “Optimum frequency of propagation in shallow water environments”, *J. Acoust. Soc. Am.*, **73**, No. 3, 813-819 (1983)

15 M.R. Schroeder, "Effect of Frequency and Space Averaging on the Transmission Responses of Multimode Media", *J. Acoust. Soc. Am.*, **46**, No. 2, 277-283 (1969)
16 R.J. Urick, *Principles of Underwater Sound*, 3rd edition, (McGraw-Hill 1983)
17 L.E. Kinsler, A.R. Frey, A.B. Coppens and J.V. Sanders, *Fundamentals of Acoustics*, 3rd Edition, (John Wiley & Sons, 1982)
18 K.L. Williams, E.I. Thorsos, and W.T. Elam, "Examination of coherent surface reflection coefficient (CSRC) approximations in shallow water propagation", *J. Acoust. Soc. America*, **116** (4), Pt. 1, 1975 – 1984 (2004)
19 M.D. Collins, "User's Guide for RAM Versions 1.0 and 1.0p", anonymous ftp@ram.nrl.navy.mil
20 Dejun, Jiang, "Complex effective depth approximation for soft solid bottom", *Chinese Journal of Acoustics*, **16**, No. 3, 260-272 (1997)
21 H. Schmidt, "OASES Version 2.1 User Guide and Reference Manual", 1997, http://oalib.hlsresearch.com/
22 I. MacGillivray, private communication (2000)
23 M.B. Porter, "*The KRAKEN Normal Mode Program*", SACLANT Undersea Research Centre (1995)